Ultrasonic study of the temperature and pressure dependences of the elastic properties of a $Mn_{78}Pt_{22}$-alloy single crystal

G. A. Saunders, M. Cankurtaran,* and P. Ray
School of Physics, University of Bath, Bath BA2 7AY, United Kingdom

J. Pelzl and H. Bach
Institut für Experimentalphysik, Ruhr-Universität Bochum, Germany

(Received 16 February 1993)

The elastic and nonlinear acoustic properties of monocrystalline $Mn_{78}Pt_{22}$ alloy have been studied by the ultrasonic pulse-echo-overlap technique. To obtain the three independent elastic-stiffness tensor components C_{IJ} and the adiabatic bulk modulus B^S as a function of temperature in the antiferromagnetic D phase, velocity measurements of the three ultrasonic modes, which can be propagated along the [110] direction, have been made between 10 K and room temperature; for the longitudinal mode measurements have been made up to 550 K. At 293 K the elastic stiffnesses are $C_{11}=94.2$ GPa, $C_{12}=35.8$ GPa, and $C_{44}=84.7$ GPa; hence C_{11} and in turn $B^S=55.2$ GPa are comparatively small: the elastic moduli conform with trends with the e/a ratio previously recognized for $3d$ transition-metal antiferromagnetic Invar alloys. In the temperature range 10–225 K the C' mode exhibits shear-lattice softening that parallels mode softening found in the longitudinal second-order elastic-stiffness tensor component C_{11}. There is a sharp dip at the Néel temperature (515 K) in the velocity of the longitudinal ultrasonic wave propagated along the [110] direction. Measurements of the hydrostatic-pressure dependences of the velocities of ultrasonic modes with a [110] propagation vector have been used to obtain the hydrostatic pressure derivatives $(\partial C_{IJ}/\partial P)_{P=0}$ of the elastic-stiffness tensor components. At 293 K $(\partial C_{11}/\partial P)_{P=0}$, $(\partial C_{12}/\partial P)_{P=0}$, $(\partial C_{44}/\partial P)_{P=0}$, and $(\partial B^S/\partial P)_{P=0}$ are 6.2±0.1, 4.2±0.3, 4.3±0.2, and 4.8±0.2, respectively. To establish the vibrational anharmonicity of the long-wavelength acoustic modes, the results obtained for C_{IJ} and $(\partial C_{IJ}/\partial P)_{P=0}$ have been used to calculate the corresponding Grüneisen parameters. In general the elastic and nonlinear acoustic properties show a number of features that resemble those of Invar materials.

I. INTRODUCTION

The objective has been to investigate the elastic and nonlinear acoustic properties of antiferromagnetic (AFM) $Mn_{78}Pt_{22}$ alloy. Measurements have been made of the temperature and hydrostatic-pressure dependences of the velocities of pure longitudinal and shear ultrasonic waves propagated along the [110] direction of a single-crystal sample. An outcome of this experimental work has been the determination of each of the independent second-order elastic-stiffness tensor components (SOEC) and related elastic properties, and how they vary with temperature and pressure. These results provide interesting physical insight into the elastic and nonlinear acoustic properties of this alloy.

An alloy with the composition $Mn_{78}Pt_{22}$ falls within the stability range (16–29 at.% Pt) of the ordered intermetallic compound Mn_3Pt.[1] The stoichiometric compound Mn_3Pt has the cubic Cu_3Au ordered structure. Previous studies of the phase centered on Mn_3Pt have been focused on its magnetic structure.[2–5] Mn_3Pt is an antiferromagnet with a Néel temperature T_N of 475 K; magnetic moments of about $3\mu_B$ are sited on the Mn atoms at 77 K, while there is no magnetic-moment alignment on the Pt atoms. Particular interest in this compound was aroused by the discovery, from neutron-diffraction studies, of a first-order transition at a temperature T_c of 365 K from one AFM phase (labeled D) to a second AFM phase (labeled F).[2–5] The crystal structure does not change at the AFM-AFM transition, but the lattice parameter increases considerably from $a_D=3.842$ Å to $a_F=3.873$ Å corresponding to a volume change $\Delta V/V$ of 2.4% and a latent heat of 1.7±0.2 cal/g. In the low-temperature ground state (D phase) the moments are coplanar, lying in {111} planes along ⟨112⟩ directions and are ordered at 120° to nearest neighbors on a triangular lattice. The unit cell is doubled in the higher-temperature AFM F phase. Recently Long[6] has pointed out that the magnetic structure proposed earlier[5] for the F phase suffers from a number of serious deficiencies and has established that it is in fact a multiple-q state comprised of an equal superposition of three spin-density waves.

The compound Mn_3Pt is isostructural with Fe_3Pt, a material which shows strong Invar effects, including negative thermal expansion in a range of temperature below the Curie point.[7] A phenomenon central to understanding this negative thermal expansion has recently been found in ultrasonic studies of the ferromagnetic Invar alloy $Fe_{72}Pt_{28}$: the application of hydrostatic pressure induces a decrease in the velocities of longitudinal ultrasonic modes.[8,9] Both $(\partial C_{11}/\partial P)_{P=0}$ and $(\partial C_L/\partial P)_{P=0}$ [where $C_L=(C_{11}+C_{12}+2C_{44})/2$)] are negative in the ferromagnetic phase, although they have the normal posi-

tive sign in the paramagnetic state. Hence below the Curie temperature the hydrostatic-pressure derivative $(\partial B/\partial P)_{P=0}$ of the bulk modulus is negative: $Fe_{72}Pt_{28}$ shows the extraordinary behavior of becoming easier to squeeze when pressure is applied to it. This fascinating behavior aroused our interest in related materials, prompting this ultrasonic study of the elastic and nonlinear acoustic properties of $Mn_{78}Pt_{22}$.

II. EXPERIMENTAL PROCEDURE

The initial obstacle to surmount was lack of information about the optimum concentration and conditions required for crystal growth. We were not able to grow a large single crystal of stoichiometric Mn_3Pt of adequate perfection for ultrasonic studies; plausibly this is due to the large volume change which takes place as a Mn_3Pt crystal is cooled through the cubic-to-cubic AFM-AFM transition. However it is possible to circumvent this difficulty. As the Mn concentration $(3+x)$ is increased in the alloy system $Mn_{3+x}Pt_{1-x}$, the lattice parameter and the jump in its value incurred as the material undergoes the first-order transition from the AFM D phase to the AFM F phase at T_c decrease, and both T_c and T_N increase.[5] The range of temperature over which the F phase is stable becomes smaller as the Mn concentration is enhanced; at a critical value of x greater than about 0.18 the F phase vanishes[5] so that the AFM-AFM transition and the associated large volume change are absent. We have concentrated our effort on growing a single crystal of an alloy of concentration $Mn_{3.12}Pt_{0.88}$ (which we express in atomic concentration as $Mn_{78}Pt_{22}$ because that has been our practice in earlier studies of Mn- and Fe-based alloys with which we compare our present work). It proved possible to grow a high-quality single crystal of this composition. When this alloy is cooled slowly through the AFM F to AFM D transition during the growth process, the volume change $\Delta V/V$ incurred is relatively small so that there is negligible strain-induced structural damage.

The single crystal of cm^3 dimensions was grown from high-purity elements by a modified Bridgman-Stockbarger process. The charge was contained in a polished alumina crucible in a high-purity argon atmosphere. Since the vapor pressure of molten manganese is high, the crucible and cover were sealed gas tight using a heat resisting adhesive for ceramics ("Ceramabond" of TEK-Hannover). This crucible was put into a Mo crucible which was welded gas tight under 300 mbar of argon. The material was heated by rf induction up to about 1250 °C, left to homogenize for an hour, and then lowered slowly down through the temperature gradient. After crystallization the cooling rate was much reduced to anneal the crystal for several days. Single crystals of about 6.5 mm diameter and 20 mm in length were grown, the crystal quality being examined by taking Laue back-reflection photographs along the boule. It has the same structure as the γ-phase compound Mn_3Pt. Microprobe analysis scans around the crystal showed its composition to be $Mn_{78}Pt_{22}$ with ± 1 at. %. The density was 7417 ± 3 $kg\,m^{-3}$. The crystal was orientated on a three-arc goniometer to $\pm 0.5°$ using Laue back-reflection photography. A sample, large enough for precision measurements of ultrasonic wave velocities, was cut and polished with two faces, normal to the required propagation direction along the [110] crystallographic axis, flat to surface irregularities of about 2 μm and parallel to better than 10^{-3} rad.

The velocities of the longitudinal and two shear pure ultrasonic waves, which can be propagated along a [110] direction, were measured. 10-MHz ultrasonic pulses were generated and detected by X- and Y-cut quartz transducers bonded to the sample using Nonaq stopcock grease at low temperatures or Dow resin above 300 K; the latter bonding agent was used in the high-pressure experiments. Ultrasonic pulse transit times were measured using the pulse-echo-overlap technique[10] capable of resolution of velocity changes to 1 part in 10^5 and particularly well suited to determination of pressure- or temperature-induced changes in velocity. The temperature dependence of the velocity of each ultrasound mode was measured between 10 and 300 K; experiments on the longitudinal mode were extended up to 550 K.

Hydrostatic pressure up to 1.5 GPa was applied in a piston-and-cylinder apparatus sealed with Teflon and Viton O rings. Silicone fluid was used as the pressure transmitting medium. The dependence of ultrasonic wave velocity upon hydrostatic pressure was measured at 293 and 333 K keeping the temperature controlled to within 0.2 K. The pressure was measured using the change in resistance of a precalibrated manganin wire coil contained inside the cell. For further details of the experimental setup, see Ref. 11. To circumvent calculation of the changes in crystal dimensions induced by application of hydrostatic pressure, the experimental data were transformed to correspond to the "natural velocity" W.[12] In decreasing order of magnitude, the major sources of error arose in the measurement of pressure, alloy composition, sample dimensions, and alignment.

III. EXPERIMENTAL RESULTS FOR THE TEMPERATURE DEPENDENCES OF THE ELASTIC-STIFFNESS TENSOR COMPONENTS OF $Mn_{78}Pt_{22}$

The adiabatic elastic-stiffness tensor components of $Mn_{78}Pt_{22}$, measured at room temperature, are compared with those of other Mn alloys and MnS_2 in Table I. The component C_{11} for each of the AFM alloys is small compared with those of Fe or Ni. This is also true for C_L. Hence the long-wavelength longitudinal acoustic phonons are relatively soft in each of these alloys, especially for $Mn_{78}Pt_{22}$. Small values are also found for the elastic stiffnesses C_{44}, C', and B^S. The results show that $Mn_{78}Pt_{22}$ conforms to the trends for $3d$ transition-metal alloys with electron concentration constructed by Lenkkeri.[16] Building on the fact that the composition dependence of the elastic moduli of alloys is associated with changes in the strain dependence of the crystal energy, he found that, as a result of the electronic contributions to the elastic moduli of an fcc transition-metal alloy, the stiffnesses and their temperature derivatives depend on

TABLE I. Comparison between the room-temperature (293 K) elastic and nonlinear acoustic properties of $Mn_{78}Pt_{22}$ and those of $Mn_{73}Ni_{27}$ (Ref. 13), $Fe_{60}Mn_{40}$ (Ref. 14), and MnS_2 (Ref. 15).

Description	$Mn_{78}Pt_{22}$	$Mn_{73}Ni_{27}$	$Fe_{60}Mn_{40}$	MnS_2
Density ($kg\,m^{-3}$)	7417		7820	3502
Elastic stiffnesses (GPa)				
C_{11}	94.2±0.1	129	170	114±1
C_{44}	84.7±0.3	98	142	36±2
C_{12}	35.8±0.1	77	98	30±2
$C'=\frac{1}{2}(C_{11}-C_{12})$	29.2±0.1	26	36	30±1
Bulk modulus B^S (GPa)	55.2±0.3	94	123	64±3
Hydrostatic-pressure derivatives				
$(\partial C_{11}/\partial P)_{P=0}$	6.2±0.1	5.2±0.1	10.1	8.9±0.1
$(\partial C_{12}/\partial P)_{P=0}$	4.2±0.3	3.2±0.3	7.1	2.8±0.2
$(\partial C_{44}/\partial P)_{P=0}$	4.3±0.1	3.5±0.1	3.8	3.9±0.1
$(\partial C'/\partial P)_{P=0}$	1.0±0.1	0.9±0.1	1.5	3.1±0.1
$(\partial B^S/\partial P)_{P=0}$	4.8±0.2	3.9±0.2	8.1	4.8±0.3
$\bar{\gamma}^{el}$	1.35	1.5	2.12	2.4

the electron/atom (e/a) ratio. At high temperatures, fcc alloys of transition metals range from γMn (e/a equal to 7) to Cu (e/a equal to 11). As e/a is decreased below 7.7 (the AFM Invar region), there is a marked tendency for the values of the elastic moduli to decrease. With an e/a ratio of 7.66, $Mn_{78}Pt_{22}$ falls into the correct place for an AFM Invar in the systematic trend found by Lenkkeri (see Fig. 1 of Ref. 16).

The temperature dependences of the adiabatic elastic moduli $C_L[=(C_{11}+C_{12}+2C_{44})/2]$, $C'[=(C_{11}-C_{12})/2]$, and C_{44} are shown in Fig. 1. These moduli refer to the AFM D phase. They were calculated from the sample density (ρ) and the velocities of ultrasonic waves propagated along the [110] direction of the $Mn_{78}Pt_{22}$ crystal as it was cooled from 300 to 10 K. There was no thermal hysteresis in the elastic moduli of the three modes and no irreversible effects, when the alloy was temperature cycled between room temperature and 10 K.

The longitudinal C_L and the shear C_{44} moduli increase smoothly with decreasing temperature and do not show any pronounced unusual effects [Figs. 1(a) and 1(b)]. These elastic moduli increase steadily in the usual way, as the temperature is decreased to about 100 K and then start to level off, reaching a temperature-independent plateau below about 50 K, behavior resembling that for these moduli in other AFM Mn alloys, such as fcc Fe-Mn (Refs. 17 and 14) and the γ Mn-Ni alloys,[18,19] which are Invars.

However, the temperature dependence between 10 and 300 K of the elastic stiffness C' associated with the $N[110]U[1\bar{1}0]$ polarized shear wave [Fig. 1(c)] is especially interesting. This elastic modulus starts to increase as the temperature is lowered from room temperature but at a small gradient: dC'/dT is only about 0.005 GPa K^{-1} at 250 K (at this temperature the gradients of the $C_L(T)$ and $C_{44}(T)$ plots are much larger, being $dC_L/dT=0.04$ GPa K^{-1} and $dC_{44}/dT=0.02$ GPa K^{-1}). With further decrease in temperature C' levels off at around 235 K and in a range centered on 200 K the gradient of the elastic modulus-temperature curve is almost zero. Then this shear stiffness begins to decrease at a rate which becomes progressively larger as the temperature is reduced further, resulting in quite a steep positive gradient in the range 150–50 K. Below 40 K, the gradient dC'/dT becomes less steep and the curve of $C'(T)$ flattens off before beginning to increase slightly at the lowest temperatures of measurement.

The elastic stiffnesses $C_{11}(=C_L+C'-C_{44})$, $C_{12}(=C_{11}-2C')$, and the adiabatic bulk modulus $B^S(=C_L-C_{44}-C'/3)$ have also been evaluated (Fig. 2). As the temperature is decreased C_{11} passes through a maximum at about 170 K and then decreases [Fig. 2(a)]. A similar longitudinal mode softening has been observed in the γ Mn-Ni alloys.[18,19] Now a decrease in C_{11} with decreasing temperature can be instrumental in reducing $(C_{11}-C_{12})/2$ in turn—as it does in γ Mn-Ni alloys.[19] The second-order stiffness tensor component C_{12} displays a more normal behavior [Fig. 2(b)]: it increases gradually as the temperature decreases before leveling off around 50 K at a value of 39.2 GPa. The adiabatic bulk modulus B^S increases slowly as the temperature is reduced from room temperature to about 120 K and then flattens out to a value just below 58 GPa in the range 50–10 K [Fig. 2(c)].

The shear anisotropy ratio $A(=C_{44}/C')$ changes from about 2.8 to 3.3 as the temperature is lowered from 293 to 10 K (Fig. 3). From 300 to 175 K, the anisotropy ratio A remains fairly constant at about 2.9. Below about 175 K, this ratio increases quite rapidly to 3.2 as the softening of the C' shear mode is enhanced [Fig. 1(c)]. The shear mode softening behavior is similar to that found for the γ Mn-Ni Invar alloys[19] and also for $Fe_{72}Pt_{28}$,[8,9] and could suggest an incipient martensitic transition, although this is not attained.

To examine some aspects of the elastic behavior of $Mn_{78}Pt_{22}$ in the vicinity of the Néel temperature, the range of measurement of the velocity of the longitudinal ultrasonic wave propagated along the [110] direction was

extended up to 550 K. The ultrasonic echoes were stable for this mode when the temperature was increased. Figure 4 shows the results obtained for the longitudinal elastic modulus C_L. At about 490 K there is a kink in $C_L(T)$, an anomaly associated with the material crossing into the F-phase existence region just below the triple point where the AFM F, and AFM D, and the paramagnetic phases coexist [see Fig. 7(b) of Ref. 20]. This $Mn_{78}Pt_{22}$ crystal is in the AFM F phase in the temperature range from 490 K up to T_N. Above 500 K, C_L decreases suddenly, reaching a deep minimum at 515 K. This should define the Néel temperature T_N for $Mn_{78}Pt_{22}$;

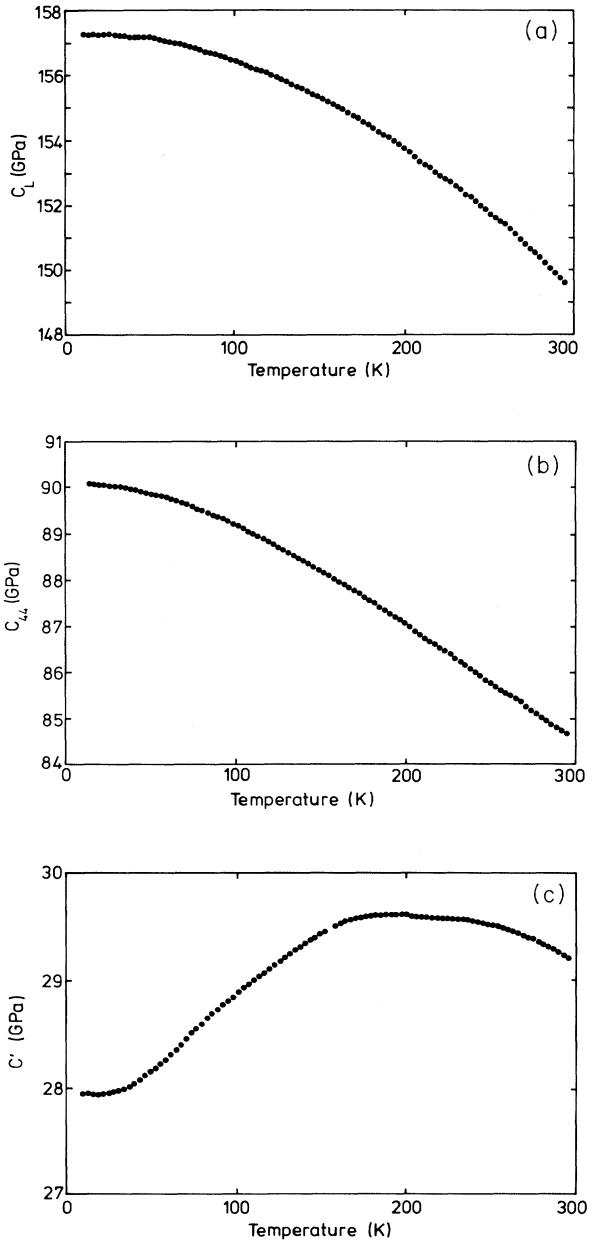

FIG. 1. Temperature dependence of the adiabatic elastic stiffnesses (a) $C_L[=(C_{11}+C_{12}+2C_{44})/2]$, (b) C_{44}, and (c) $C'[=(C_{11}-C_{12})/2]$ of $Mn_{78}Pt_{22}$ in the AFM D phase.

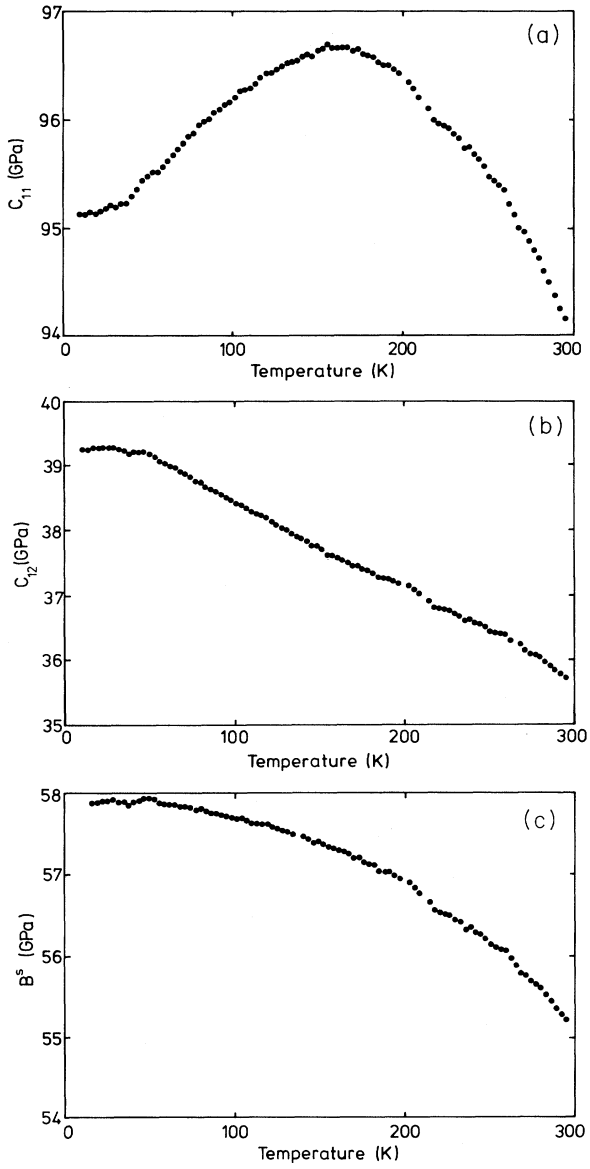

FIG. 2. Temperature dependence of the adiabatic elastic stiffnesses (a) C_{11} and (b) C_{12} and (c) the bulk modulus B^S of $Mn_{78}Pt_{22}$ in the AFM D phase.

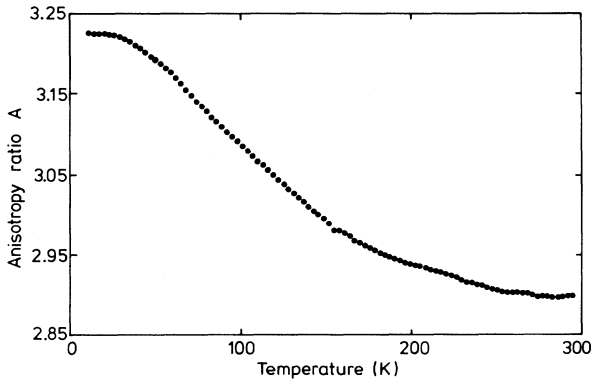

FIG. 3. Variation of the shear anisotropy ratio $A(=C_{44}/C')$ for $Mn_{78}Pt_{22}$ in the AFM D phase with decreasing temperature.

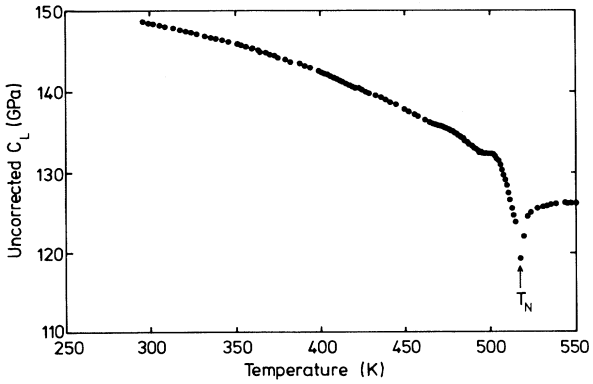

FIG. 4. Longitudinal elastic stiffness $C_L[=(C_{11}+C_{12}+2C_{44})/2]$ of $Mn_{78}Pt_{22}$ as a function of temperature. The data were obtained during warming.

a similar dip occurs at T_N in the case of $Fe_{60}Mn_{40}$.[14] The neutron-diffraction studies gave a value of 502 ± 10 K for T_N for an alloy of composition $Mn_{78}Pt_{22}$.[2–5,20] Above T_N the longitudinal elastic modulus increases sharply before leveling out by about 530 K.

IV. DISCUSSION OF THE TEMPERATURE DEPENDENCES OF THE ELASTIC-STIFFNESS TENSOR COMPONENTS OF $Mn_{78}Pt_{22}$ IN THE AFM *D* PHASE

When $Mn_{78}Pt_{22}$ is cooled down from room temperature to 10 K, the elastic stiffnesses C_L and C_{44} [Figs. 1(a) and (b)] show no obvious evidence for softening or any other characteristic which might be linked with Invar-type behavior. These two independent elastic stiffnesses follow approximately the temperature dependence common to antiferromagnetic alloys, such as, for example, those observed in γ Mn-Ni (Refs. 18 and 19) and γ Fe-Mn (Refs. 21, 17, and 14) alloys.

By contrast, the velocity of the shear C' mode does exhibit interesting features [Fig. 1(c)]. At first glance, the temperature dependence of C' seems to resemble the behavior for this shear stiffness found for the ferromagnetic Invar alloy $Fe_{65}Ni_{35}$.[21] The mode softening occurring in the range from 200 to 10 K could be construed as evidence either for Invar behavior or for an incipient martensitic transition. In fact the two properties can be interlinked. Softening of the C' mode is typical antiferromagnetic Invar effect[19,22,14] and also occurs in many ferromagnetic Invar materials (for a review, see Ref. 22). Thus, in conjunction with the results obtained for $C_{11}(T)$ [Fig. 2(a)], the $C'(T)$ temperature dependence for the $Mn_{78}Pt_{22}$ alloy displays behavior resembling that of an Invar alloy, although the Invar-like characteristics are not as pronounced as those of ferromagnetic alloys such as, for instance, $Fe_{72}Pt_{28}$ (Refs. 8, 9, and 14) and $Fe_{65}Ni_{35}$.[21]

Since C_{11} and C_L are relatively small, compared with those of Fe or Ni, for example, the implication is that the long-wavelength longitudinal phonons are soft. There is a magnetoelastic interaction which softens C_{11} below 200 K [Fig. 2(a)]. In turn this is paralleled by softening of C' and since this modulus is small, the effect is most pronounced in its temperature dependence. This observation resembles the effects noted in the elastic constant results for γ Mn-Ni alloys.[18,19]

Comparison between the elastic behaviors of $Mn_{78}Pt_{22}$ and antiferromagnetic $Mn_{85}Ni_{15}$ (Ref. 18) indicates the same general pattern. C_L goes through a quite a sharp minimum at T_N, which is 465 K for $Mn_{85}Ni_{15}$ and 515 K for $Mn_{78}Pt_{22}$. Apart from the dip near T_N for the longitudinal C_L mode in $Mn_{85}Ni_{15}$, the magnetic ordering induces a stiffening in the rest of the temperature range; very similar behavior is found for $Mn_{78}Pt_{22}$, which, however, shows in addition the feature at 490 K attributable to the *D*-to-*F* transition. On closer examination, the elastic behavior displayed as a function of temperature by $Mn_{78}Pt_{22}$ is similar to $Mn_{85}Ni_{15}$,[18] and also to the "classic" ferromagnetic Fe-Ni (Ref. 21) and Fe-Pt (Refs. 23 and 24) Invar alloys in which the effects are much more pronounced while in the manganese-rich, antiferromagnetic Invar alloys and $Fe_{60}Mn_{40}$ alloy,[14] they are less so. The magnitudes of the magnetoelastic and Invar effects are usually much smaller for an antiferromagnetic alloy than for a ferromagnetic alloy.

V. THE HYDROSTATIC-PRESSURE DEPENDENCES OF THE ULTRASONIC WAVE VELOCITIES AND ELASTIC-STIFFNESS TENSOR COMPONENTS OF $Mn_{78}Pt_{22}$ IN THE AFM *D* PHASE

The pressure dependences of the ultrasonic wave velocities for the longitudinal C_L mode and the two shear C' and C_{44} modes were measured. The velocities associated with the three independent elastic-stiffness moduli increase approximately linearly with pressure at room temperature (Fig. 5). The data are reproducible under pressure cycling and show no hysteresis effects. The hydrostatic-pressure derivatives $(\partial C_{IJ}/\partial P)_{P=0}$, in the zero pressure limit, of $Mn_{78}Pt_{22}$ at 293 K are given in Table I. They were almost the same at 333 K.

It is instructive to compare these results for $(\partial C_{IJ}/\partial P)_{P=0}$ with those for other alloys, especially those containing manganese, to see whether any parallels can be drawn and any trends observed. Table I shows data obtained for $Mn_{78}Pt_{22}$, together with those for $Mn_{73}Ni_{27}$,[13] $Fe_{60}Mn_{40}$,[14] and a compound MnS_2 in the high-spin state.[15] The hydrostatic-pressure derivatives of the SOEC's for $Mn_{78}Pt_{22}$ all have positive values, like those of $Mn_{73}Ni_{27}$. This is also the case for $Fe_{60}Mn_{40}$ (Ref. 14) and MnS_2.[15]. The elastic stiffnesses and thus the slopes of the acoustic-mode dispersion curves, at the long-wavelength limit, increase with pressure in the normal way. The application of pressure does not induce acoustic-mode softening for any of these AFM manganese-containing materials.

A common trend for cubic crystals is that

$$(\partial C_{11}/\partial P)_{P=0} > (\partial C_{44}/\partial P)_{P=0} > (\partial C'/\partial P)_{P=0} .$$

For each of the materials, which are compared in Table I,

the largest pressure derivative is $(\partial C_{11}/\partial P)_{P=0}$, implying that the higher-order elastic effects are dominated by nearest-neighbor repulsive forces. A striking feature for $Mn_{73}Ni_{27}$ of the temperature dependences of the hydrostatic-pressure derivatives of the SOEC's is that there is substantial increase in all of them with temperature, especially in $(\partial C_{11}/\partial P)_{P=0}$.[13] This is not the case for $Mn_{78}Pt_{22}$; as the temperature is increased to 333 K, there is very little change in the value of $(\partial C_{11}/\partial P)_{P=0}$. This different behavior could possibly be explained by the fact that the platinum atoms play a minimal role in the magnetic structure in $Mn_{78}Pt_{22}$. The magnetic properties affect the structure and characteristics of any compound, and in the case of $Mn_{73}Ni_{27}$, both elements contribute to the fundamental magnetic makeup of the alloy.

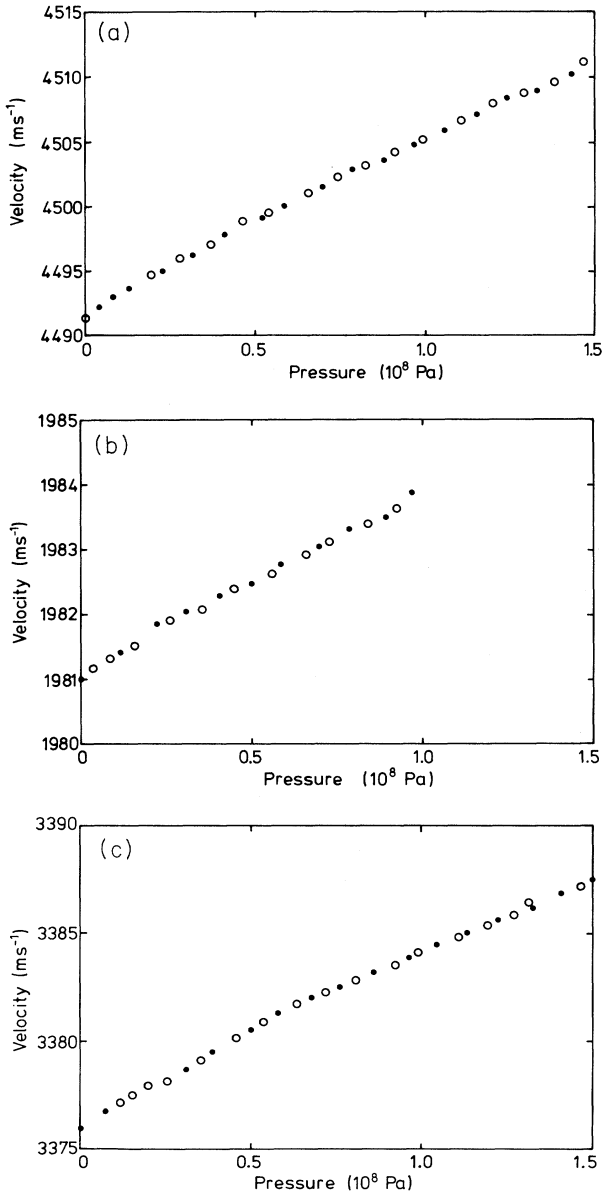

FIG. 5. Hydrostatic-pressure dependences of the velocities of (a) the longitudinal C_L mode, (b) the shear $C'[=(C_{11}-C_{12})/2]$ mode, and (c) the shear C_{44} mode of $Mn_{78}Pt_{22}$ in the AFM D phase at room temperature (293 K). The filled circles correspond to ultrasonic wave velocity measurements made as the pressure was increased and the open circles as the pressure was decreased.

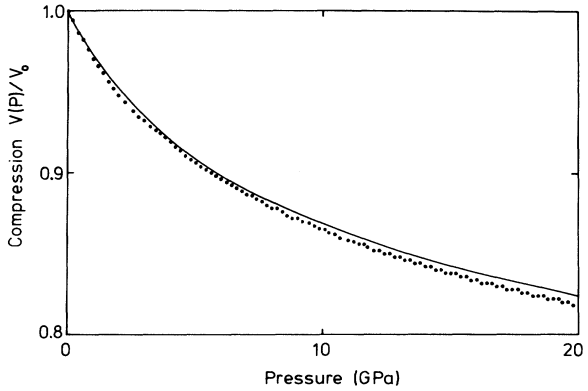

FIG. 6. Volume compression of $Mn_{78}Pt_{22}$ extrapolated to very high pressures using Murnaghan's equation of state (Ref. 25) at 293 K (line) and 333 K (filled circles).

The measurements of the elastic stiffnesses and their hydrostatic-pressure dependences have been used to calculate the volume compression $V(P)/V_0$ of $Mn_{78}Pt_{22}$ up to very high pressures, using an extrapolation method based on the Murnaghan[25] equation of state in the logarithmic form. The calculation has been performed for the data at 293 and 333 K; the results are shown in Fig. 6. In the absence of thermal expansion and specific-heat data, B^S has been used rather than B^T throughout the calculation. The magnitude of the volume compression for $Mn_{78}Pt_{22}$ is typical of that for a transition-metal Invar alloy.

VI. GRÜNEISEN PARAMETERS AND THE ACOUSTIC-MODE VIBRATIONAL ANHARMONICITY OF $Mn_{78}Pt_{22}$

To a large extent the Invar properties of an alloy are determined by the anharmonicity of its vibrational states.[8,9,14] Measurements of the elastic-stiffness tensor components and their hydrostatic-pressure derivatives can be used to determine the acoustic-mode Grüneisen parameters at the long-wavelength limit which quantify the vibrational anharmonicity of these particular modes. In the case of volume change induced by an applied hydrostatic pressure, the acoustic-mode Grüneisen parameter γ_p in a phonon branch p of a cubic crystal can be calculated using[26]

$$\gamma_p = -\frac{1}{6w_p}[3B + 2w_p + k_p] , \tag{1}$$

where

$$w_p = C_{11}k_1 + C_{44}k_2 + C_{12}k_3 ,$$

and

$$k_p = -k_1\left[C_{11}+3B+3B\left(\frac{\partial C_{11}}{\partial P}\right)_T\right]$$
$$-k_2\left[C_{44}+3B+3B\left(\frac{\partial C_{44}}{\partial P}\right)_T\right]$$
$$-k_3\left[C_{12}-3B+3B\left(\frac{\partial C_{12}}{\partial P}\right)_T\right]$$

with

$$k_1 = N_1^2U_1^2+N_2^2U_2^2+N_3^2U_3^2 ,$$
$$k_2 = (N_2U_3+N_3U_2)^2+(N_3U_1+N_1U_3)^2$$
$$+(N_1U_2+N_2U_1)^2 ,$$
$$k_3 = 2(N_2N_3U_2U_3+N_3N_1U_3U_1+N_1N_2U_1U_2) .$$

Here N_i and U_i $(i=1,2,3)$ are the direction cosines of the wave propagation and the particle displacement directions, respectively. The acoustic-mode Grüneisen parameters, computed at 293 K, are shown in Fig. 7 as a function of the propagation direction. The Grüneisen parameters are rather small in the branch which includes the $N[110]U[1\bar{1}0]$ polarized soft shear mode. The behaviors of the acoustic-mode Grüneisen parameters for $Mn_{78}Pt_{22}$ resemble those of the AFM Invar alloy $Fe_{60}Mn_{40}$,[14] in that the longitudinal mode gammas are larger than those of the shear modes and the mode gammas in a given branch do not vary substantially with propagation direction. The mean long-wavelength acoustic-mode Grüneisen parameter $\bar{\gamma}^{el}$ calculated for $Mn_{78}Pt_{22}$ is found to have a normal value (Table I). The thermal Grüneisen parameter cannot be calculated because neither the specific-heat capacity nor the thermal expansion are available.

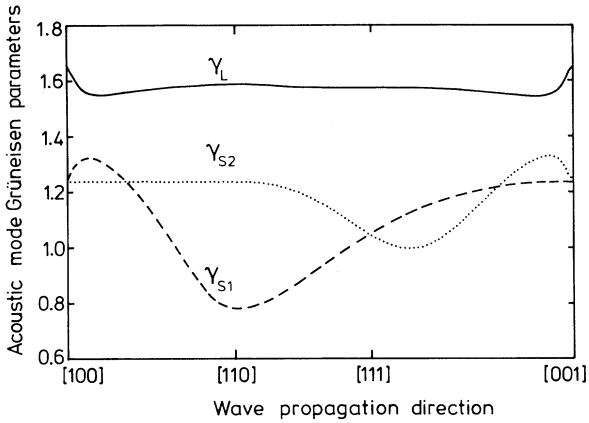

FIG. 7. Long-wavelength, longitudinal (solid line), and shear (dashed and dotted lines) acoustic-mode Grüneisen parameters of $Mn_{78}Pt_{22}$ in the AFM D phase as a function of mode propagation direction at 293 K.

VII. CONCLUSIONS

The velocities of the three ultrasonic modes propagated along the [110] direction of the AFM $Mn_{78}Pt_{22}$ single-crystal alloy have been measured as functions of temperature and hydrostatic pressure. The data have been used to determine the temperature dependences of the elastic-stiffness tensor components C_{IJ} and the adiabatic bulk modulus B^S and their pressure derivatives $(\partial C_{IJ}/\partial P)_{P=0}$ and $(\partial B^S/\partial P)_{P=0}$. There are several interesting features to note, which shed light on the elastic, nonlinear acoustic and lattice dynamical properties of $Mn_{78}Pt_{22}$. They can be summarized as follows:

(i) The C' mode exhibits shear-lattice softening in the temperature range 10–225 K. This follows the behavioral pattern for antiferromagnetic γ Mn-Ni Invar alloys. This can be linked with the observation that the longitudinal SOEC C_{11} is small and shows enhanced mode softening below 170 K. In contrast, softening has not been established in either the longitudinal C_L mode or the shear C_{44} stiffness. This is also in keeping with antiferromagnetic Invar behavior typified by γ Mn-Ni alloys and $Fe_{60}Mn_{40}$.

(ii) The shear anisotropy ratio A changes in accordance with the changes in C'.

(iii) The Néel temperature has been determined as 515 K from the position of a sharp minimum observed in the velocity of the longitudinal ultrasonic wave propagated along the [110] direction and hence in the corresponding elastic modulus C_L.

(iv) A kink observed in the temperature dependence of C_L at 490 K indicates the temperature at which this alloy undergoes the AFM-to-AFM transition; this crystal is in the AFM F phase between 490 K and T_N.

(v) $Mn_{78}Pt_{22}$ is a comparatively soft material elastically. Its elastic moduli fit into the trends with e/a ratio established for AFM Invar alloys.

(vi) The acoustic-mode Grüneisen parameters at room temperature have normal values but significantly are small in the branch which includes the soft C' mode.

*Permanent address: Hacettepe University, Department of Physics, 06532 Ankara, Turkey.

[1] *Metallography, Structures and Phase Diagrams,* Vol. 8 of *Metals Handbook,* 8th ed. (American Society for Metals, Ohio, 1973), p. 317.

[2] E. Kren, G. Kadar, L. Pal, J. Solyom, and P. Szabo, Phys. Lett. **20**, 331 (1966).

[3] E. Kren, G. Kadar, L. Pal, and P. Szabo, J. Appl. Phys. **38**, 1265 (1967).

[4] E. Kren, P. Szabo, L. Pal, T. Tarnoczi, G. Kadar, and C. Hargitai, J. Appl. Phys. **39**, 469 (1968).

[5] E. Kren, G. Kadar, L. Pal, J. Solyom, P. Szabo, and T. Tarnoczi, Phys. Rev. **171**, 574 (1968).

[6] M. W. Long, J. Phys. Condens. Matter **3**, 7091 (1991).

[7] K. Sumiyama, M. Shiga, M. Morioka, and Y. Nakamura, J. Phys. F **9**, 1665 (1979).

[8] Ll. Mañosa, G. A. Saunders, H. Radhi, U. Kawald, J. Pelzl, and H. Bach, J. Phys. Condens. Matter **3**, 2273 (1991).

[9]Ll. Mañosa, G. A. Saunders, H. Radhi, U. Kawald, J. Pelzl, and H. Bach, Phys. Rev. B **45**, 2224 (1992).
[10]E. P. Papadakis, J. Acoust. Soc. Am. **42**, 1045 (1967).
[11]S. C. Flower and G. A. Saunders, Philos. Mag. B **62**, 311 (1990).
[12]R. N. Thurston and K. Brugger, Phys. Rev. **133**, A1604 (1964).
[13]G. A. Saunders and M. D. Salleh, Philos. Mag. (to be published).
[14]M. Cankurtaran, G. A. Saunders, P. Ray, Q. Wang, U. Kawald, J. Pelzl, and H. Bach, Phys. Rev. B **47**, 3161 (1993).
[15]G. A. Saunders, Wang Qingxian, E. F. Lambson, N. Lodge, D. Paine, and W. Hönle, J. Phys. Condens. Matter **2**, 3713 (1990).
[16]J. T. Lenkkeri, J. Phys. F **11**, 1997 (1981).
[17]J. T. Lenkkeri, J. Phys. F **11**, 1991 (1981).
[18]G. Hausch and E. Török, J. Magn. Magn. Mater. **6**, 269 (1977).
[19]R. D. Lowde, R. T. Harley, G. A. Saunders, M. Sato, R. Scherm, and C. Underhill, Proc. R. Soc. London Ser. A **374**, 87 (1981).
[20]H. Yasui, T. Kaneko, H. Yoshida, S. Abe, K. Kamigaki, and N. Mori, J. Phys. Soc. Jpn. **56**, 4532 (1987).
[21]Ph. Renaud, Ph.D. thesis, Université de Lausanne, Switzerland, 1988.
[22]E. F. Wassermann, in *Ferromagnetic Materials,* edited by K. H. J. Buschow and E. P. Wohlfarth (North-Holland, Amsterdam, 1990), Vol. V, p. 237.
[23]G. Hausch, J. Phys. Soc. Jpn. **37**, 819 (1974).
[24]U. Kawald, W. Zemke, H. Bach, J. Pelzl, and G. A. Saunders, Physica B **161**, 72 (1989).
[25]F. D. Murnaghan, Proc. Nat. Acad. Sci. USA **30**, 244 (1944).
[26]K. Brugger and T. C. Fritz, Phys. Rev. **157**, 524 (1967).